

# We are IntechOpen, the world's leading publisher of Open Access books Built by scientists, for scientists

6,900

Open access books available

186,000

International authors and editors

200M

Downloads

Our authors are among the

154

Countries delivered to

TOP 1%

most cited scientists

12.2%

Contributors from top 500 universities



WEB OF SCIENCE™

Selection of our books indexed in the Book Citation Index  
in Web of Science™ Core Collection (BKCI)

Interested in publishing with us?  
Contact [book.department@intechopen.com](mailto:book.department@intechopen.com)

Numbers displayed above are based on latest data collected.  
For more information visit [www.intechopen.com](http://www.intechopen.com)



---

# Atmospheric Propagation Model for Satellite Communications

---

Ali Mohammed Al-Saegh, A. Sali, J. S. Mandeep, Alyani Ismail,  
Abdulmajeed H.J. Al-Jumaily and Chandima Gomes

Additional information is available at the end of the chapter

<http://dx.doi.org/10.5772/58238>

---

## 1. Introduction

As the radio frequency signal radiates through an Earth-sky communication link, its quality degrades as it propagates through the link because of the absorption and scattering by the particles in space [1]. This degradation significantly affects the received information, particularly with the recent advances in satellite technologies and services, which require a high information rate. Furthermore, the extent of degradation depends on the link, atmospheric, transmitted signal, and receiver antenna parameters.

Two types of signal fluctuations caused by atmospheric phenomena, fast and slow fluctuations [2], as shown in Figure 1. The former is called scintillation, which is typically caused by rapid variations of signal performance attributed to the turbulent refractive index inhomogeneity in the medium. Meanwhile, slow fluctuations are usually caused by the absorption and scattering of the signal energy by the particles, particularly water droplets, in the link between the satellite and the earth station.

With respect to the atmospheric layers, the satellite signal may be subjected to different types of scintillations. Ionospheric scintillation occurs because of the irregularities in electron density in the ionosphere [3] (approximately from 85 km to 600 km above sea level) and, thus, irregularities in the refractive index. Whereas, tropospheric scintillation is caused by irregularities in radio refractivity as the wave travels along different medium densities in the troposphere (approximately 0 km to 10 km above sea level) [2].

The variation of the transmitted signal parameters (frequency  $f$  and elevation angle  $\theta$ , in particular) has the major impact on the amount of the atmospheric impairments. For the transmitted signal frequencies below 3 GHz, the ionospheric scintillation has a significant

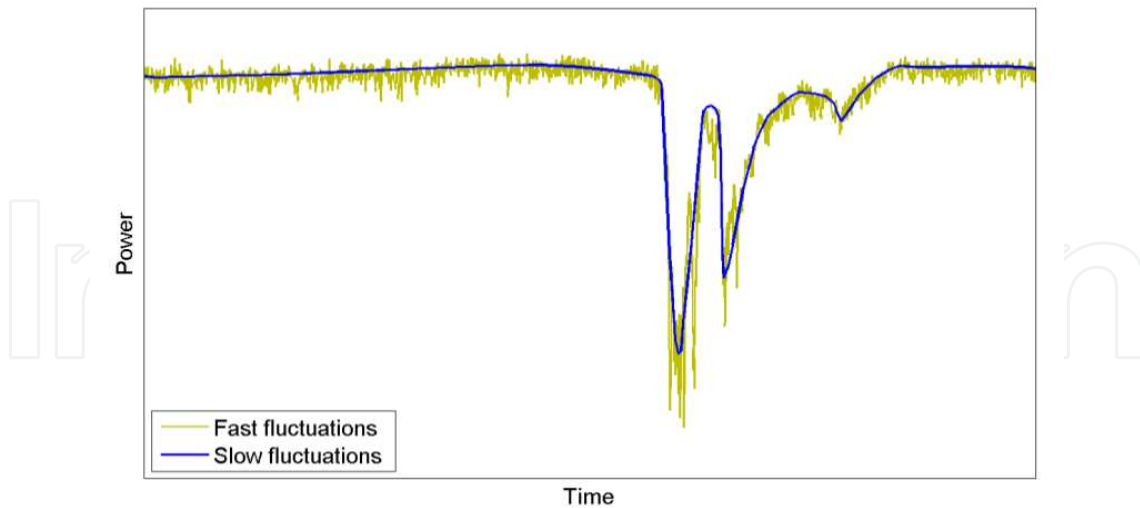


**Figure 1.** Fast and slow fluctuations

effect. However, this phenomenon becomes negligible as the frequency increases [4]. Consequently, for frequencies above 10 GHz, other phenomena, such as rain and clouds, impose a serious impact on the signal attenuation [5]. The oxygen and water vapor particles in space have a significant effect at higher signal frequencies [3].

Transmission at a low-elevation angle during the rain, condensed clouds, water vapor and Oxygen will increase the effective rain, clouds, water vapor, and Oxygen path of the signal on the medium, respectively, which in turn causes degradation in the received signal level. Therefore, the engineers in earth stations try to access the nearest possible satellite in order to increase the elevation angle, and hence, decrease the effect of atmospheric parameters.

The atmospheric impairments effects on the earth sky communication quality increase the need for developing prediction models in order to index the atmospheric fade level as well as select the proper fade mitigation technique (FMT).

This chapter proposes a complete model of atmospheric propagation to improve the estimation and the analysis of atmospheric effects on the signal quality in satellite communications using actual measured parameters. The model is composed of correlated modules that include channel modules and quality assessment extended modules.

## 2. Channel model

The general satellite system model contains three main components: Earth station(s), satellite(s), and the link(s) between them (channel/s). The channel and receiver models have been built using MATLAB as explained in the following subsections.

The satellite link may suffer from poor signal quality owing to atmospheric impairments. Raindrops cause significant effect at higher transmission frequencies, particularly above 10

GHz [5]. Other atmospheric phenomena, such as clouds, water vapor, and oxygen, significantly affect signal attenuation, especially at higher transmission frequencies. The models were implemented in Matlab based on the radiowave sector recommendations from the International Telecommunication Union (ITU) which proved to be suitable for satellite communications.

## 2.1. Rain attenuation

Rain droplets absorb and scatter the signal energy and cause its power level to attenuate to a value depending on the size, amount, and shape of the droplets that the signal passes through as well as the rain rate [6]. Rain usually occurs at different heights above sea level depending on a region on the earth.

Several rain attenuation prediction models have been developed which gained world agreements, such as Crane [7], group of researchers from International Telecommunication Union-Radiowave sector (ITU-R) [8, 9], DAH [10], and SAM [11]. These models were developed through many years of monitoring and observations. However, less than 5% of annual time usually contains rainy events. ITU-R [8] used this percentage as a starting point for their rain attenuation prediction model. To recognize the characteristics of rainy conditions in any area in the world, a percentage of less than 1% of the time of the year, which includes the rainfall that causes a significant amount of attenuation as the signal propagated through, is required to be taken into consideration.

The rain attenuation model shown in Figure 2 has been built and implemented based on modified ITU-R prediction model. In Particular, the actual measured rain rate in [6], rather than the predicted values by the ITU-R model, has been applied to construct a more accurate rain estimation model. The model has been implemented using Matlab. The initialization contains values for earth station position parameters (latitude, and height above sea level), rain parameters (rain rate, rain height, and percentage of exceedance time  $p$ ), and transmitter parameters (frequency  $f$ , elevation angle  $\theta$ , and polarization angle  $\tau$ ).

The developed program performs two procedures simultaneously. The first procedure starts with obtaining the frequency-dependent rain attenuation empirical values [12] before calculating the rain specific coefficients  $k$  and  $\alpha$  through Eq. (1) and (2).

$$k = \frac{k_H + k_V + (k_H - k_V) \cos^2 \theta \cos (2 \tau)}{2} \quad (1)$$

$$\alpha = \frac{k_H \alpha_H + k_V \alpha_v + (k_H \alpha_H - k_V \alpha_v) \cos^2 \theta \cos (2 \tau)}{2k} \quad (2)$$

The rain specific attenuation (the rain attenuation per 1 km) is then calculated using Eq. (3) depending on the actual measured rainfall rate (at  $p=0.01\%$ ) listed in [6] rather than the ITU predicted values in [9].

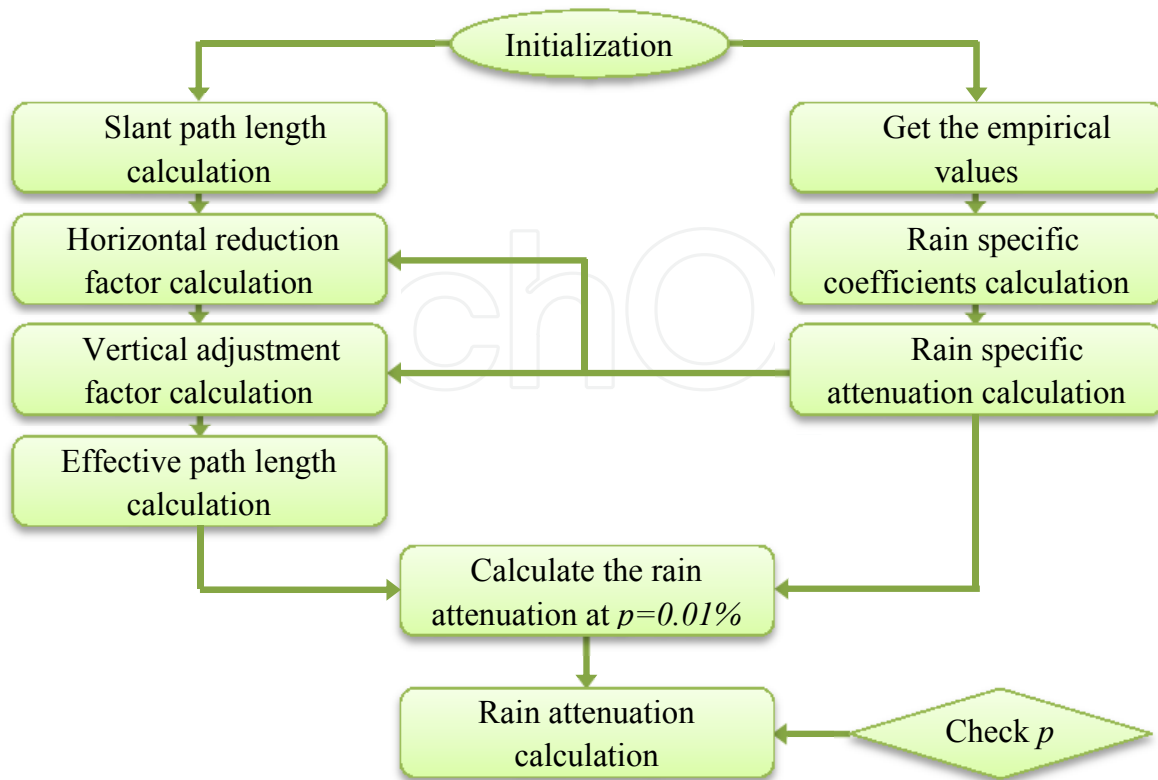


Figure 2. Rain attenuation model

$$\gamma_{Rain} = \alpha(R_{0.01})^k \tag{3}$$

This value will be used in the second procedure to identify the effective path length as well as to predict the overall rain attenuation. The horizontal reduction factor ( $r_H$ ) for 0.01% of the time can be calculated using Eq. (4).

$$r_H = \frac{1}{1 + 0.78 \sqrt{\frac{P_H \gamma_R}{f} - 0.38(1 - e^{-2P_H})}} \tag{4}$$

where  $P_H$  is the horizontal projection which depends on the slant path length and the elevation angle, as imposed by Eq. (5)

$$P_H = L_S \cos \theta \tag{5}$$

The slant path length depends on the vertical height from the earth station to the rain height as well as on  $\theta$ , as shown in Eq. (6).

$$L_S = \begin{cases} \frac{H_R - H_S}{\sin \theta} & \text{for } \theta \geq 5^\circ \\ \frac{2(H_R - H_S)}{\sqrt{\sin^2 \theta + \frac{2(H_R - H_S)}{E_R} + \sin \theta}} & \text{for } \theta < 5^\circ \end{cases} \quad (6)$$

where  $H_R$  and  $H_S$  are the rain and earth station heights above sea level, respectively; and  $E_R$  is the earth radius (8500 km). The vertical adjustment factor ( $V_F$ ) can be calculated at 0.01% of the time using Eqs. (7) to (9).

$$\xi = \tan^{-1} \left( \frac{H_R - H_S}{P_H r_H} \right) \quad (7)$$

$$L_R = \begin{cases} \frac{P_H r_H}{\cos \theta} & \text{for } \xi > \theta \\ \frac{H_R - H_S}{\sin \theta} & \text{for } \xi \leq \theta \end{cases} \quad (8)$$

$$V_F = \frac{1}{1 + \sqrt{\sin \theta} \left[ 31 \left( 1 - e^{-\frac{\theta}{1-x}} \right) \frac{\sqrt{L_R \gamma_R}}{f^2} - 0.45 \right]} \quad (9)$$

where  $x$  depends on the latitude ( $\varphi$ ) of the earth station. The calculation of the horizontal reduction and vertical adjustment factors in the ITU-R model is based on 0.01% of the time exceedance because these factors actually indicate the temporal variability of rain drop dimension and rain height, respectively [13]. The effective path length can be obtained using Eq. (10), whereas the total rain attenuation at 0.01% of time ( $A_{0.01}$ ) can be calculated using Eq. (11).

$$L_E = L_R V_F \quad (10)$$

$$A_{0.01} = L_E \gamma_R \quad (11)$$

Consequently, the predicted rain attenuation at any percentage of time ( $p$ ) can be calculated using Eqs. (12) and (13).

$$\beta = \begin{cases} 0 & \text{If } p \geq 1\% \text{ or } |\varphi| \geq 36^\circ \\ -0.005(|\varphi| - 36) & \text{If } p < 1\% \text{ and } |\varphi| < 36^\circ \text{ and } \theta \geq 25^\circ \\ -0.005(|\varphi| - 36) + 1.8 - 4.25 \sin \theta & \text{Otherwise} \end{cases} \quad (12)$$

$$A_{rain} = A_{0.01} \left( \frac{p}{0.01} \right)^{-[0.655 + 0.033 \ln(p) - 0.045 \ln(A_{0.01}) - \beta(1-p) \sin \theta]} \quad (13)$$

The signal performance during rain events at different transmission parameters is analyzed along with received signal strength and error rates assessments.

## 2.2. Cloud attenuation

The cloud content of liquid water also causes absorption and scattering of electromagnetic energy especially for frequencies above 10 GHz, but with less intensity than that of rain [6]. Cloud attenuation, in addition to the transmission parameters such as the signal frequency and the elevation angle  $\theta$ , depends on the cloud parameters such as average height and thickness, as well as the total columnar content of liquid water in Kg/m<sup>2</sup> (liquid water contents *LWC*) and temperature.

Several models have been developed to estimate cloud attenuation, such as Salonen & Uppala [14], ITU-R [15], DAH [16], and Altshuler & Marr [17]. Salonen & Uppala and ITU-R are identical in terms of the procedure used to predict the cloud attenuation, as shown in Figure 3. The only difference between these two models is in the prediction of the *LWC*.

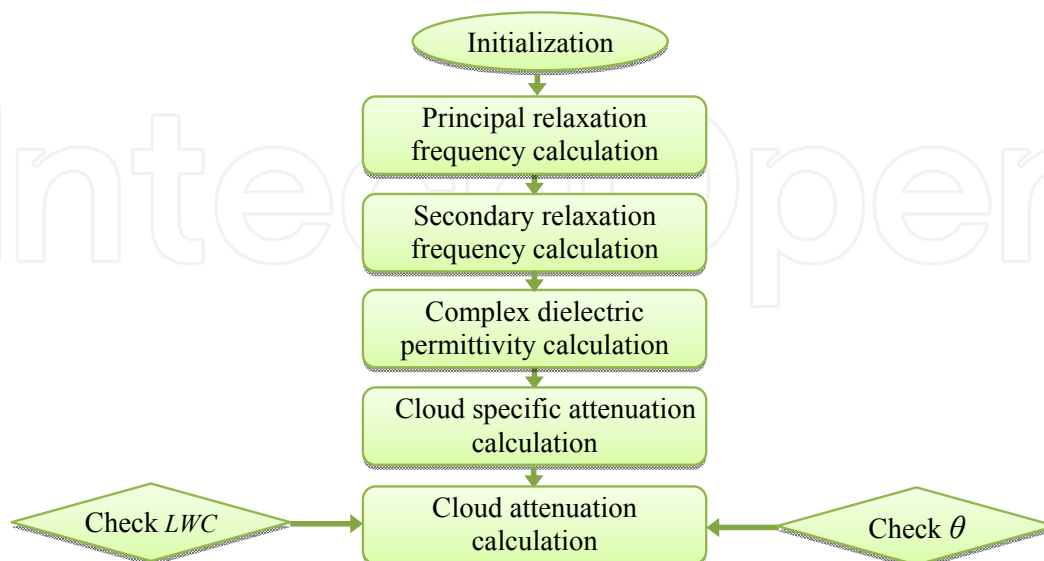


**Figure 3.** Cloud attenuation model

The cloud attenuation estimation model has been implemented based on the Salonen & Uppala and ITU-R models. The implemented model started with the initialization of the aforementioned parameters.

The principal and secondary relaxation frequencies are calculated using Eqs. (14) and (15), respectively.

$$f_{r_{pri}} = 20.09 - 142(\Lambda - 1) + 294(\Lambda - 1)^2 \quad (14)$$

$$f_{r_{sec}} = 590 - 1500(\Lambda - 1) \quad (15)$$

where  $\Lambda = 300/T$ , and  $T$  is the temperature in Kelvin. The complex dielectric permittivity of water contents in the cloud is given by:

$$\varepsilon' = \frac{\varepsilon_0 - \varepsilon_1}{1 + \left(\frac{f}{f_{r_{pri}}}\right)^2} + \frac{\varepsilon_1 - \varepsilon_2}{1 + \left(\frac{f}{f_{r_{sec}}}\right)^2} + \varepsilon_2 \quad (16)$$

$$\varepsilon'' = \frac{f(\varepsilon_0 - \varepsilon_1)}{f_{r_{pri}} \left[1 + \left(\frac{f}{f_{r_{pri}}}\right)^2\right]} + \frac{f(\varepsilon_1 - \varepsilon_2)}{f_{r_{sec}} \left[1 + \left(\frac{f}{f_{r_{sec}}}\right)^2\right]} \quad (17)$$

where  $\varepsilon_0 = 77.6 + 103.3(\Lambda - 1)$ , whereas  $\varepsilon_1$  and  $\varepsilon_2$  are equal to 5.48 and 3.51, respectively. However, the cloud specific attenuation coefficient can be calculated using Eq. (18).

$$\gamma_{clouds} = \frac{0.819f}{\varepsilon'' \left[1 - \left(\frac{2 + \varepsilon'}{\varepsilon''}\right)^2\right]} \quad (18)$$

The cloud attenuation at any probability depends on the  $LWC$  that can be obtained from radiosonde or radiometric measurements for the region of interest.

$$A_{clouds} = \gamma_{clouds} \left(\frac{LWC}{\sin \theta}\right) \quad (19)$$

However, the  $LWC$  can be predicted using either Salonen & Uppala [14] or ITU-R study group 3 [15] prediction values. The former implies that  $LWC$  is obtained from a proposed map depending on the temperature and height from the cloud base. The latter implies the use of

the annual values of  $LWC$  exceeded at some specific locations for several percentages of annual time from digital maps they proposed containing  $LWC$  values. The values for other desired locations on Earth can be derived by interpolation.

### 2.3. Water vapor and oxygen attenuations

The signal propagating through the atmosphere undergoes a degradation in signal level owing to the water vapor and dry air components in the transmission medium [18]. Water particles absorb and scatter the wave energy more than oxygen.

Water vapor attenuation depends on the weather parameters such as temperature, water vapor content, and altitude above sea level. The attenuation increases proportionally once the temperature and relative humidity (RH) increase. However, oxygen has the paramount effect among all other gases because the dry atmosphere contains 20.946% oxygen, thus resulting in a significant effect on satellite wave frequencies above 50 GHz [3, 19]. The oxygen attenuation analysis differs from other atmospheric impairments, because its effect on all the regions on the earth remains constant and independent.

Numerous experiments have been conducted [19, 20] using radiosonde for the purpose of observing and predicting the water content and oxygen attenuation. However, the ITU-R propagation sector came up with a prediction model [21] that has gained global agreement.

Figures. 4(a) and (b) shows the water vapor and oxygen attenuation models, respectively. The models, which have been implemented based on the ITU-R approximate estimation model, were initialized with related parameters such as the transmitted frequency, relative humidity, mean temperature, and pressure.

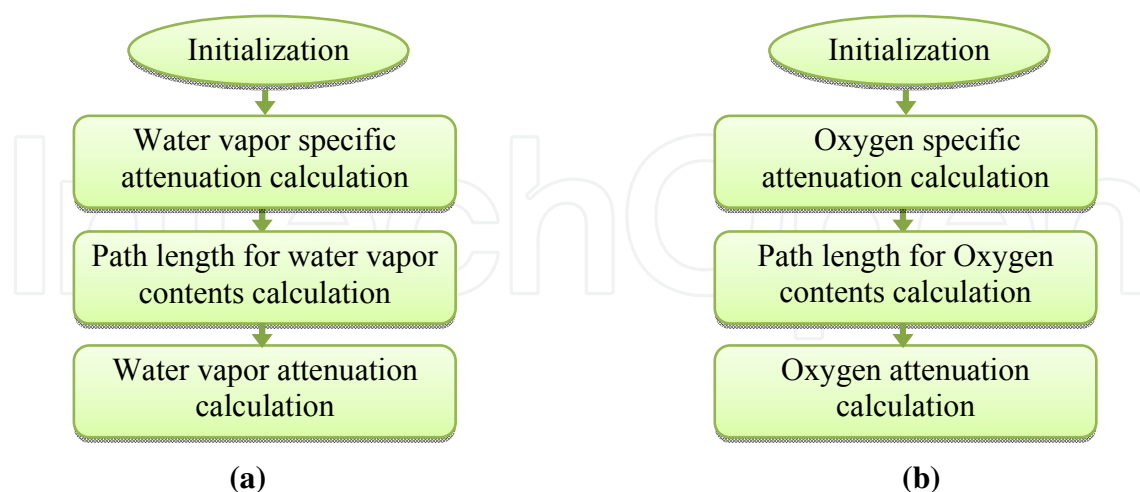


**Figure 4.** Water vapor and oxygen attenuation models (a) water vapor, and (b) oxygen

Oxygen specific attenuation can be determined for frequencies up to 350 GHz from the equations listed in Table 1.

Frequency (GHz)	Equation
$f \leq 54$	$\gamma_O = f^2 r_p^2 \left[ \frac{7.2 r_T^{2.8}}{f^2 + 0.34 r_p r_T^{1.6}} + \frac{0.62 \xi_3}{(54 - f)^{1.16 \xi_2}} \right] \times 10^{-3}$
$54 < f \leq 60$	$\gamma_O = \exp \left[ \frac{\ln g_{54}}{24} (f - 58)(f - 60) - \frac{\ln g_{58}}{8} (f - 54)(f - 60) + \frac{\ln g_{60}}{12} (f - 54)(f - 58) \right]$
$60 < f \leq 62$	$\gamma_O = g_{60} + \frac{f - 60}{2} (g_{62} - g_{60})$
$62 < f \leq 66$	$\gamma_O = \exp \left[ \frac{\ln g_{62}}{8} (f - 64)(f - 66) - \frac{\ln g_{64}}{4} (f - 62)(f - 66) + \frac{\ln g_{66}}{8} (f - 62)(f - 64) \right]$
$66 < f \leq 120$	$\gamma_O = f^2 r_p^2 \left[ 3.02 \times 10^{-4} r_T^{3.5} \frac{0.283 r_T^{3.8}}{(f - 118.75)^2 + 2.91 r_p^2 r_T^{1.6}} + \frac{0.502 \xi_6 (1 - 0.0163 f \xi_7 - 1.0758 \xi_7)}{(f - 66)^{1.4346 \xi_4} + 1.15 \xi_5} \right] \times 10^{-3}$
$120 < f \leq 350$	$\gamma_O = f^2 r_p^2 r_T^{3.5} \left[ \frac{3.02 \times 10^{-4}}{1 + 1.9 \times 10^{-5} f^{1.5}} + \frac{0.283 r_T^{0.3}}{(f - 118.75)^2 + 2.91 r_p^2 r_T^{1.6}} \right] \times 10^{-3} + \delta$

**Table 1.** Oxygen specific attenuation calculation [21]

Where  $r_p$  and  $r_T$  are coefficients related to pressure ( $r_p = \text{Pressure}/1013$ ) and temperature ( $r_T = 288/T$ ) respectively.  $\xi_n$ ,  $g_n$  and  $\delta$  can be obtained from [21]. The path length for oxygen content can be determined using Eq. (20).

$$L_O = \frac{6.1(1 + z_1 + z_2 + z_3)}{1 + 0.17 r_p^{-1.1}} \quad (20)$$

where

$$z_1 = \frac{4.64}{1 + 0.066 r_p^{-2.3}} \exp \left[ - \left( \frac{f - 59.7}{2.87 + 12.4 \exp(-7.9 r_p)} \right)^2 \right] \quad (a)$$

$$z_2 = \frac{0.14 \exp(2.12 r_p)}{(f - 118.75)^2 + 0.031 \exp(2.2 r_p)} \quad (b) \quad (21)$$

$$z_3 = \frac{0.0114 f}{1 + 0.14 r_p^{-2.6}} \left( \frac{-0.0247 + 0.0001 f + 1.61 \times 10^{-6} f^2}{1 - 0.0169 f + 4.1 \times 10^{-5} f^2 + 3.2 \times 10^{-7} f^3} \right) \quad (c)$$

Meanwhile, Eq. (22) is used to calculate the water vapor specific attenuation in (dB/km).

$$\gamma_W = f^2 r_T^{2.5} \rho [s_1 + s_2 + s_3 + s_4 + s_5 + s_6 + s_7 + s_8 + s_9] \times 10^{-4} \tag{22}$$

Where  $\rho$  is the water vapor density in (g/m<sup>3</sup>).  $S_{1..9}$  can be obtained from Table 2.

Par	Equation	Par	Equation
$S_1$	$\frac{3.98\eta_1 \exp[2.23(1-r_T)]}{(f-22.235)^2 + 9.42\eta_1^2} \left[ 1 + \left( \frac{f-22}{f+22} \right)^2 \right]$	$S_6$	$\frac{17.4\eta_1 \exp[1.46(1-r_T)]}{(f-448)^2}$
$S_2$	$\frac{11.96\eta_1 \exp[0.7(1-r_T)]}{(f-183.31)^2 + 11.14\eta_1^2}$	$S_7$	$\frac{844.6\eta_1 \exp[0.17(1-r_T)]}{(f-557)^2} \left[ 1 + \left( \frac{f-557}{f+557} \right)^2 \right]$
$S_3$	$\frac{0.08\eta_1 \exp[6.44(1-r_T)]}{(f-321.226)^2 + 6.29\eta_1^2}$	$S_8$	$\frac{290\eta_1 \exp[0.41(1-r_T)]}{(f-752)^2} \left[ 1 + \left( \frac{f-752}{f+752} \right)^2 \right]$
$S_4$	$\frac{3.66\eta_1 \exp[1.6(1-r_T)]}{(f-325.153)^2 + 9.22\eta_1^2}$	$S_9$	$\frac{8.3328 \times 10^4 \eta_2 \exp[0.99(1-r_T)]}{(f-1780)^2} \cdot \left[ 1 + \left( \frac{f-1780}{f+1780} \right)^2 \right]$
$S_5$	$\frac{25.37\eta_1 \exp[1.09(1-r_T)]}{(f-380)^2}$	$\eta_1$	$0.955r_p r_T^{0.68} + 0.006\rho$
		$\eta_2$	$0.735r_p r_T^{0.5} + 0.0353r_T^4 \rho$

**Table 2.** Water vapor density calculation [21]

The effective path length may vary with respect to season, latitude, and/or climate change. However, the ITU-R estimated the effective water vapor path length in the troposphere for  $f \leq 350$  GHz using Eq. (23).

$$L_W = 1.66 \left( \frac{1 + \frac{1.39\sigma_W}{(f-22.235)^2 + 2.56\sigma_W}}{\frac{3.37\sigma_W}{(f-183.31)^2 + 4.69\sigma_W} + \frac{1.58\sigma_W}{(f-325.1)^2 + 2.89\sigma_W}} \right) \tag{23}$$

where

$$\sigma_W = \frac{1.013}{1 + \exp(4.902 - 8.6r_p)} \tag{24}$$

The effective water vapor path length is based on the assumption of an exponential atmosphere to describe the relation between water vapor density and altitude. At this point, the total gases attenuation  $A_{Gases}$  (oxygen and water vapor attenuations) can be predicted using Eq. (25).

$$A_{Gases} = \frac{A_O + A_W}{\sin \theta} = \frac{\gamma_O L_O + \gamma_W L_W}{\sin \theta} \quad (25)$$

### 3. Extended model

The extended model has been added to improve the signal quality assessment in satellite communication networks for several modulation schemes to propose the optimal *FMT*. According to the Friis transmission equation [18, 22], the received power in dB is the summation of the power transmitted  $P_T$ , the antenna gains of the transmitter  $G_T$ , and the receiver  $G_R$ , and the subtraction of the losses. The link losses are composed of two types, namely, the free space loss (*FSL*), and the atmospheric losses. The *FSL*, which depends on the link distance ( $d$ ) and transmitted frequency  $f=(3 \times 10^8)/\lambda$ , can be calculated using Eq. (26).

$$FSL = 20 \log \left( \frac{4\pi d}{\lambda} \right) \quad (26)$$

The atmospheric losses discussed in Section 2 are the second type of link losses. The received carrier power-to-noise ratio is estimated to identify the total degradation of the power in dB. The total noise depends on the bandwidth, in addition to the system and antenna noise temperatures. Based on the Friis transmission equation and to analyze the communication signal quality, the bit energy-to-noise ratio  $E_b/N_o$  can be calculated using Eq. (27).

$$E_b/N_{o,dB} = EIRP + G_r - FSL - L_A - L_S - N_o - 10 \log(R_b) \quad (27)$$

where *EIRP* is the Effective Isotropic Radiated Power; and  $L_A$ ,  $L_s$ ,  $N_o$  and  $R_b$  are the atmospheric losses, system losses, noise spectral density, and bit rate, respectively. The atmospheric impairments negatively affect the data after being demodulated in the receiver. The effects appear as a decrease in  $E_b/N_o$  and bit error rate (*BER*). These two metrics are used in selecting the optimal *FMT* at the time instants. The *BER* caused by atmospheric impairments can be approximated based on a Gray-code using Eq.28 [23].

$$BER \approx \frac{SER}{\log_2(M)} \quad (28)$$

where the symbol error rate (*SER*) is calculated using the equations listed in [6] for three modulation schemes: QPSK, 8-PSK and 16-PSK. The extended model has been added in order to improve the signal quality assessment in satellite communication networks for several modulation schemes to propose the optimal FMT. The extension includes several steps in the receiver side of the system, and comprises the calculation of the received signal power with the extraction of the atmospheric effects,  $E_b/N_o$  that indicates the signal quality, and *BER*.

#### 4. Indexing and FMT

Recent satellite communications technologies make massive use of resource management procedures such as channel state reporting and *FMT*. The procedure for channel state reporting (indexing) is a fundamental feature of satellite networks utilizing *FMT* since it enlists the estimated channel quality level at the receiver, and then send this report to the transmitter to apply specific technique in the next period of time. Each index is calculated as a quantized and scaled measure of the experienced  $E_b/N_o$ ,  $E_s/N_o$ , *BER* or *SER*. The reported values can be used to make decisions concerning the resource allocation to users experiencing specific channel conditions or application of a certain *FMT*. In TDM/TDMA transmitters, the decision is applied for a time period called transmission time interval (*TTI*). For every *TTI*, the allocation decision or *FMT* is performed with a validation until the next *TTI*.

*FMT* is usually classified into two types [6]. The first type mainly deals with a variation in signal characteristics (such as Adaptive coding and modulation ACM, time diversity, or frequency diversity). The second type does not concern the signal modifications (such as power control, or site diversity).

The reporting procedure is related to the *FMT* module, which selects the proper modulation and coding scheme in a case where a satellite network use the ACM technique for the process of maximizing the supported throughput with a given target error rate. Therefore, a user experiencing higher  $E_b/N_o$  will be served with higher bitrates, whereas a user experiencing poor channel conditions, will be served with lower bitrates to maintain active connections with lower error bits. It is worth to mention that the number of modulation and coding schemes is limited. Therefore, the throughput is upper-bounded over a specific threshold and the increase in the  $E_b/N_o$  does not result in any gain in throughput. This is the main reason of applying ACM technique accompanied with the power control technique.

The power control technique (uplink or downlink power control) is a dynamic procedure that adjusts transmission power to compensate for instantaneous channel condition variations [24]. These adjustments reduce power while maintaining a constant bitrate, or boost power to decrease losses when a higher modulation and coding scheme are selected, thus, increasing the bitrate. Henceforth, the aim is to keep the expected error rate below a target threshold.

However, some satellite networks consist of two or more ground stations spatially separated by at least 20 km [25] to provide separate propagation paths to the signal. This technique is called site diversity. The idea is to provide two different satellite channels that will not be significantly affected by rain attenuation simultaneously. This process enables the use of the best channel condition with a higher received signal level.

The transmitted signal can also be repeated at different time frames. Therefore, the receiver will receive more than one copy of the data transmitted. This technique is called time diversity. The time separation between successive repetitions should be greater than the channel coherence time to prevent the correlation of the received signals. Finally, frequency diversity involves transmitting the same message simultaneously at sufficiently separated (more than the coherence bandwidth) transmitted frequencies.

## 5. Complete proposed propagation model

The complete proposed propagation model for the satellite network is shown in Figure 5. The model consists of three parts: the transmitter, channel, and receiver. The modules in the channel and the receiver are the main concern of this chapter.

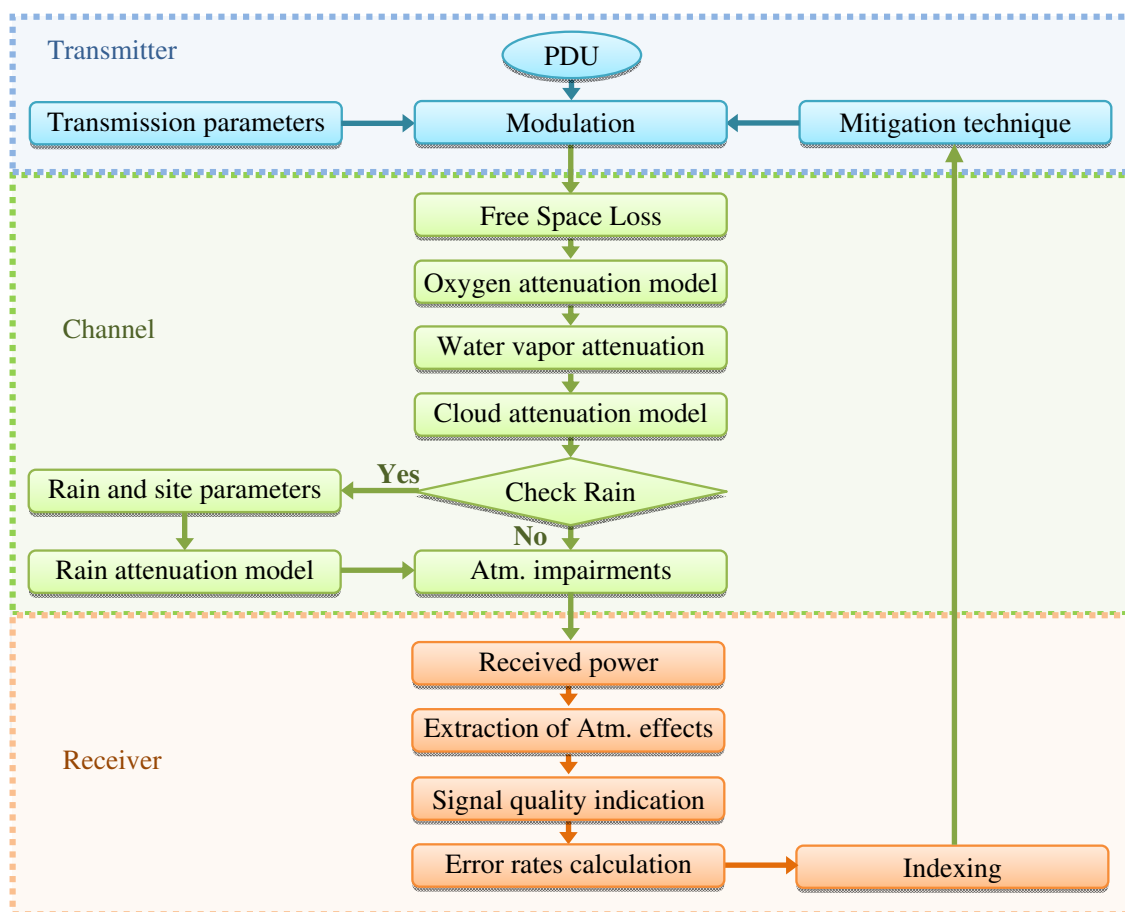


**Figure 5.** Complete propagation model

The packet data units are transmitted using specific transmission parameters and mitigation technique selected through the reported satellite channel. The effect of FSL, dry air (oxygen), and water vapor attenuation are added before the cloud attenuation module. The

availability of rain attenuation is then checked. The rain and position parameters are also identified for the purpose of determining the effect of rain to the signal power. The total atmospheric impairments are then calculated to evaluate the received signal power as mentioned in section 3.

The atmospheric impairments and their effects on the received signal signified by  $E_b/N_o$  are then evaluated at different elevation angles.  $E_b/N_o$  is used for the signal quality indication and BER evaluation at different modulation schemes. The obtained values are then indexed in the process of estimating the instantaneous satellite channel quality. These values are then reported to the transmitter for the selection of the appropriate FMT to the next TTI. The model has been applied and the results were obtained at specific modules with signal evaluation and assessment under different atmospheric and transmission parameters.

## 6. Results and discussion

The frequency of the satellite signal transmitted during rain events has a significant effect on the amount of signal power attenuation as shown in Figure 6. The analysis involved a satellite terminal located in Selangor, Malaysia (Latitude 3.01 N, Longitude 101.6 E), and the  $\theta$  was fixed to  $45^\circ$ . It is clearly shown that the 6 GHz C-band transmitted frequency has very low amount of attenuation even at heavy rain events (0.01% of time).

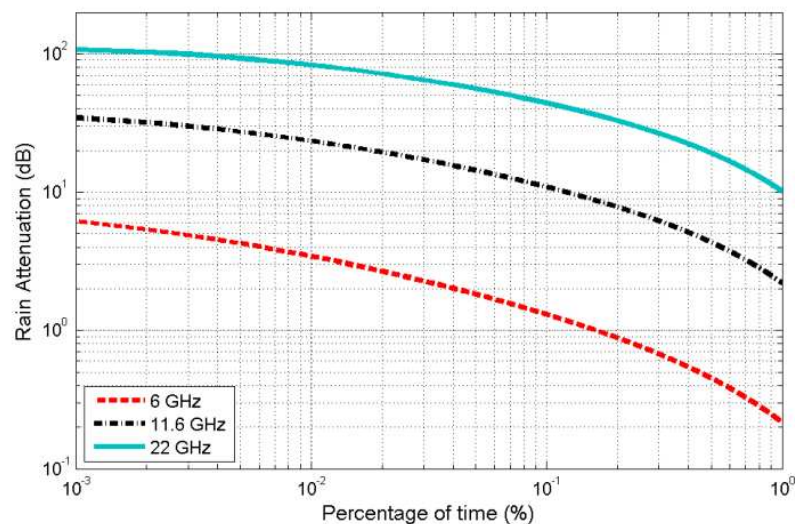


**Figure 6.** Rain attenuation at different percentages of time and frequencies

At 11.6 GHz Ku-band frequency, the rain attenuation at 0.01% of time ( $A_{0.01}$ ) is approximately 23.4 dB and reached approximately 34.5 dB at 0.001% of the time, whereas  $A_{0.01}$  reached approximately 83 dB if the signal was transmitted at 22 GHz Ka-band carrier frequency. The elevation angle is a highly effective parameter for the signal quality degradation. Figure 7 shows the amount of rain attenuation at different frequencies and elevation angles.

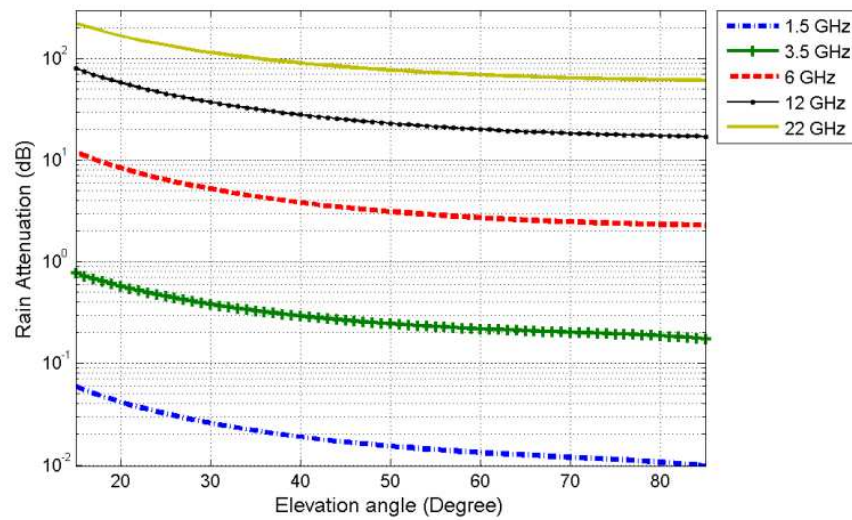


**Figure 7.** Rain attenuation at different  $\theta$  and  $f$

During rain events, the transmission link elevation angle is inversely proportional to the effective rain path of the signal and hence the amount of rain attenuation, whereas the transmitted frequency is directly proportional to the rain attenuation value. Consequently, the satellite position in space and the earth station terminal identifies the  $\theta$  of the communication link. With the aid of the results in Figure7, the rain attenuation at three different satellites connected to earth station in Selangor has been analyzed as shown in results listed in table 3 for several frequencies.

Satellite	Elevation angle ( $\theta$ )	Rain attenuation (dB)				
		1.5GHz L-Band	3.5 GHz S-Band	6 GHz C-Band	12 GHz Ku-Band	22 GHz Ka-Band
MEASAT 3/3A (91.5° E)	77.5°	0.01	0.2	2.36	17.6	62.5
SUPERBIRD C2 (144° E)	41.1°	0.02	0.29	3.73	27.3	88.7
INTLESAT 19 (166° E)	17.4°	0.05	0.67	9.93	67.8	191

**Table 3.** Rain attenuation at different satellites and transmission frequencies

It's obvious that there is a difference in the amount of rain attenuation at the same frequency but with different satellite (different  $\theta$ ). Consequently, there is a significant change in rain attenuation as the frequency band changed for the same satellite (fixed  $\theta$ ).

For cloud attenuation, the transmitted frequency and amount of liquid water in the cloud have a major effect on signal power attenuation. Figure 8 displays these effects on the amount of cloud attenuation.

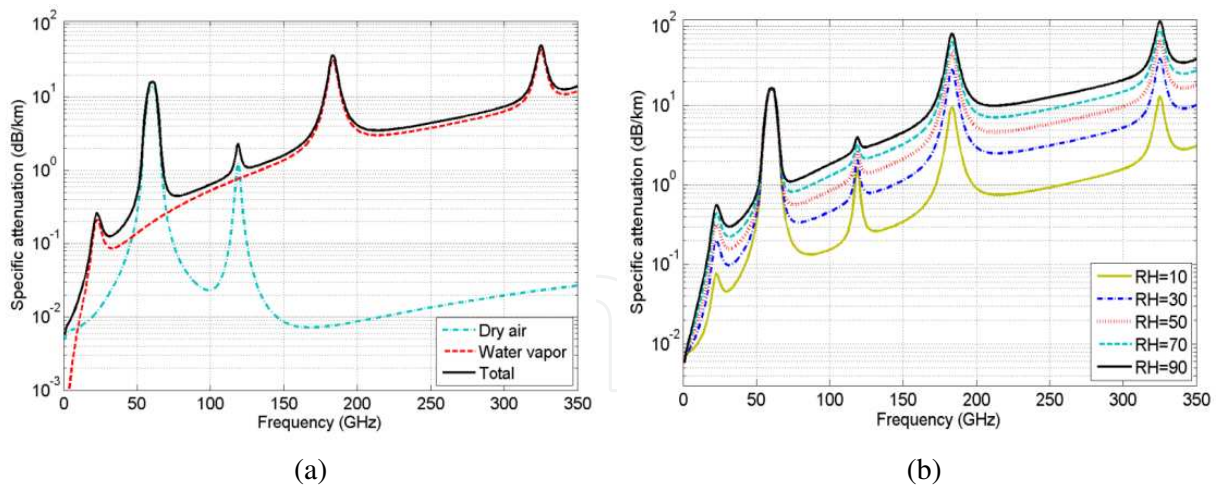


Figure 9. Gases attenuation.

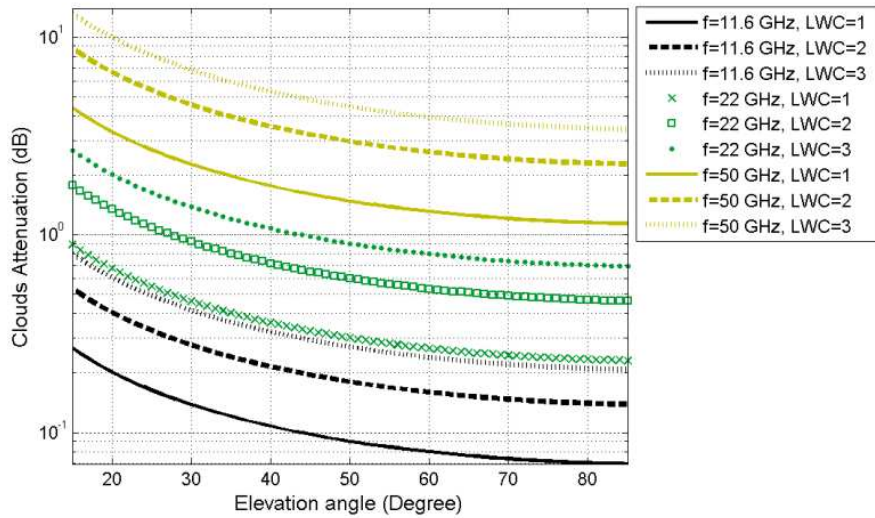


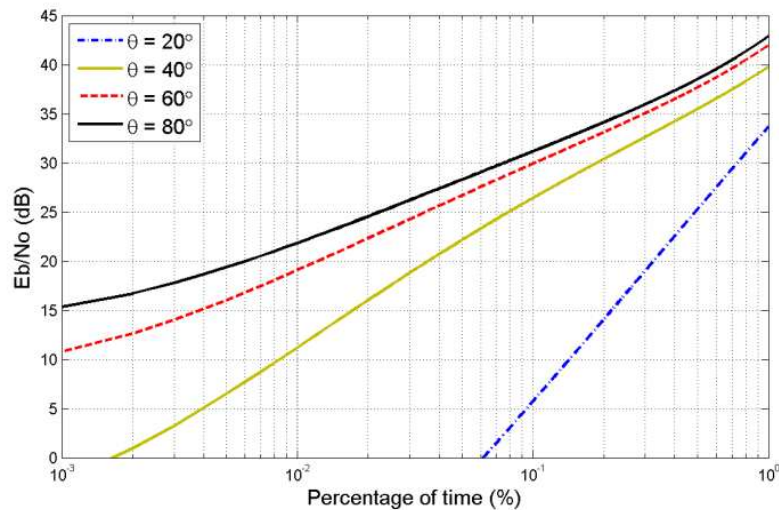
Figure 8. Cloud attenuation at different  $f$ ,  $\theta$ , and  $LWC$

Figure 8 shows that the effect of clouds at Ku band frequencies is almost negligible for all  $\theta$  and  $LWC$ , whereas the cloud attenuation at 22 GHz Ka frequency band are below 1 dB for a different  $LWC$  at  $\theta > 45^\circ$ , and below 3 dB for lower  $\theta$  at 2 and 3  $\text{Kg/m}^2$   $LWC$ . At 50 GHz V frequency band, a significant amount of cloud attenuation exceeding 10 dB for  $LWC=3$   $\text{Kg/m}^2$  and  $\theta$  below  $20^\circ$  was observed. Whereas it reached 1.8 dB, 3.6 dB, and 5.3 dB for  $\theta=41.1^\circ$  and  $LWC$  was 1, 2, and 3  $\text{Kg/m}^2$ , respectively. Consequently, cloud attenuation reached approximately 1.17 dB, 2.3 dB, and 3.5 dB if the if  $\theta=77.5^\circ$  and  $LWC$  was 1, 2, and 3  $\text{Kg/m}^2$ , respectively.

The significant amount of dry air and water vapor specific attenuation appears at specific regions across the frequency spectrum, and hence the total correlated gases attenuation, as shown in Figure 9(a)

The significant specific attenuation started at frequencies above 55 GHz mainly due to the effect of oxygen, and then the attenuation level went down. The effect appeared again at frequencies above 170 GHz, but this time mainly due to water vapor attenuation. The gases attenuation at fixed 40% RH reached higher level at approximately 325 GHz. The relative humidity (RH) is directly proportional to the amount of signal power attenuation due to the water vapor particles in space, and hence the total gases attenuation as shown in Figure 9b. However, the regions near the sea and the equator usually suffer from higher RH which indicates increased gases attenuation.

The channel quality level can be identified by the value of  $E_b/N_o$ . This leads to the selection of the proper FMT for the next TTI. The channel quality during atmospheric impairments is varied according to several parameters.  $\theta$  is one of the major parameters that specify the channel quality during atmospheric dynamics. Figure 10 shows the  $E_b/N_o$  with various rainfall events at different  $\theta$  for 11.6 GHz transmitted frequency.



**Figure 10.** Bit energy to noise ratio for different  $\theta$

The higher the elevation angle, the lower the attenuation and therefore the higher the value of  $E_b/N_o$ . During very heavy rain (around 0.001% of annual time), bad channel quality imposes serious problems to the users of the satellite networks. This leads to communication link outage at lower  $\theta$ . The BER calculations depends on the  $E_b/N_o$  along with the transmission bit rate and bandwidth. Figure 11 shows the BER approximated for three modulation schemes: QPSK, 8-PSK, and 16-PSK.

As the number of bits per second increased with the M-ary<sup>1</sup> modulation scheme, the number of error bits increased simultaneously during the signal propagation through the atmosphere. For rainy weather events, the higher the M-ary modulation scheme, the higher the BER due to

<sup>1</sup> M-ary is a term derived from the word binary. M represents a digit that corresponds to the modulation order. M=4, 8, and 16 for the QPSK, 8-PSK, and 16-PSK modulation schemes, respectively. more details in [26].

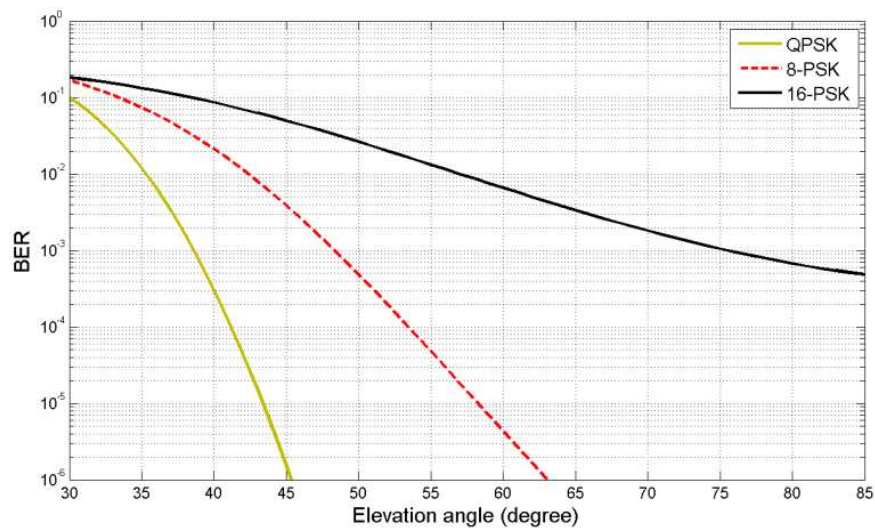


**Figure 11.** Bit error rate

the higher number of transmitted bits in unit time. Consequently, Figure 10 also clarifies that the  $\theta$  is inversely proportion to  $BER$ . QPSK modulation can be considered the most appropriate modulation scheme in case of high atmospheric impairments, but at the cost of a lower number of transmitted bits per unit time.

## 7. Conclusion

This chapter presented the atmospheric impairments to the satellite signal quality in terms of performance evaluation and assessments concerning various effective atmospheric and transmission parameters during dynamic weather conditions. The impairments presented were caused by rain, clouds, dry air (oxygen), and water vapor attenuation. An overview of ionospheric and tropospheric scintillations, channel status reporting (indexing), and FMT was provided. The atmospheric propagation model was introduced. The model included a transmitter, channel, and receiver modules built using Matlab which was revealed to be appropriate for building mathematical and analytical models. Channel conditions were evaluated along with quality and error rate estimation extensions. The atmospheric impairments results were obtained based on actual measured real-world parameters. The performance analysis of the proposed extended and propagation modules for the satellite system included atmospheric attenuation, signal-to-noise ratios, bit energy-to-noise ratios, as well as BER. The results showed that the rain attenuation effect started at frequencies above 10 GHz and exhibited the largest effects among other atmospheric phenomena, followed by cloud attenuation, and gases attenuation that have the least effects. Moreover, the results revealed that the transmitted frequency, rainfall rates,  $LWC$ , and relative humidity are directly proportional to the signal quality degradation, whereas  $\theta$  is inversely proportional. The reported channel quality, which indicated by  $E_b/N_o$ , under poor

conditions may suffer from link outage at heavy rain events for low  $\theta$ . This condition corresponds to low BER, particularly at a higher M-ary modulation scheme. The chapter would be useful for satellite system designer to accurately predict the atmospheric impairments that may affect the channel, and identifying signal quality performance with error rates during weather dynamics.

## Appendix: Matlab code

```

%-----
% Initialization
%-----
% Input parameters:
% The values of these parameters can be adjusted according to the scenario or region of interest.

% Transmission parameters
disp('Transmission parameters:');
command = 'Input the elevation angle (Degree): ';
Elev = input(command);
if Elev<5 || Elev>90
    error('please input value from 5 to 90 ')
end
command = 'Input the transmission frequency (GHz): ';
f=input(command);
if f<0.1 || f>350
    error('please input value from 0.1 to 350 ')
end
command = 'Input the polarization? (1 for Horizontal, 2 for Vertical, and 3 for Circular): ';
pol= input(command);
if pol==1
    tau=0;
elseif pol==2
    tau=90;
elseif pol==3
    tau=45;
else
    error('please input integers from 1 to 3 ')
end
disp('-----');

% Atmospheric parameters
disp('Atmospheric parameters:');
command = 'Input percentage of exceedance time (from 0.001% to 5%): ';
P = input(command);
command = 'Input Rain Rate for 0.01% of time (mm/h): ';
Rrate = input(command);
% Some actual measured rain rate values can be obtained from [6].
command = 'Input Rain height above sea level (km): ';
hR = input(command);
command = 'Input liquid water contents LWC (Kg/m^2): ';
LWC = input(command);
command = 'Input Temperature (K): ';
T = input(command);
command = 'Input the relative humidity (%): ';
RH = input(command);

```

```

if RH<0 || RH>100
    error('please input value from 0 to 100')
end
command = 'Input pressure (hPa): ';
p = input(command);
disp('=====');

% Satellite and earth station parameters
disp('Satellite and earth station parameters:');
command = 'Input the Effective Isotropic radiated power (dBW): ';
EIRP = input(command);
command = 'Input earth station Latitude : ';
Lat = input(command);
command = 'Input Station height above sea level (km): ';
hs = input(command);
command = 'Input receiver gain (dBi): ';
gr = input(command);
disp('=====');

%-----
% Rain attenuation
%-----

% Frequency-dependent rain attenuation empirical values (K and alpha)
% In order not to take much space, the empirical values are defined here for
% frequency range from 11 to 14 GHz
% other frequency values can be obtained from ITU-R P.838 recommendation.
% Source: http://www.itu.int/dms\_pubrec/itu-r/rec/p/R-REC-P.838-3-200503-I!!PDF-E.pdf
if f==11
    kH=0.01772;
    kV=0.01731;
    alphaH=1.2140;
    alphaV=1.1617;
elseif f<12 && f>11
    kH=((f-11)/(12-11))*(0.02386-0.01772)+0.01772;
    kV=((f-11)/(12-11))*(0.02455-0.01731)+0.01731;
    alphaH=((f-11)/(12-11))*(1.1825-1.2140)+1.2140;
    alphaV=((f-11)/(12-11))*(1.1216-1.1617)+1.1617;
elseif f==12
    kH=0.02386;
    kV=0.02455;
    alphaH=1.1825;
    alphaV=1.1216;
elseif f<13 && f>12
    kH=((f-12)/(13-12))*(0.03041-0.02386)+0.02386;
    kV=((f-12)/(13-12))*(0.03266-0.02455)+0.02455;
    alphaH=((f-12)/(13-12))*(1.1586-1.1825)+1.1825;
    alphaV=((f-12)/(13-12))*(1.0901-1.1216)+1.1216;
elseif f==13

```

```

kH=0.03041;
kV=0.03266;
alphaH=1.1586;
alphaV=1.0901;
elseif f<14 && f>13
kH=((f-13)/(14-13))*(0.03738-0.03041))+0.03041;
kV=((f-13)/(14-13))*(0.04126-0.03266))+0.03266;
alphaH=((f-13)/(14-13))*(1.1396-1.1586))+1.1586;
alphaV=((f-13)/(14-13))*(1.0646-1.0901))+1.0901;
elseif f==14
kH=0.03738;
kV=0.04126;
alphaH=1.1396;
alphaV=1.0646;
% Update the frequency-dependent rain attenuation empirical values here
end

k=(kH+kV+((kH-kV)*((cosd(Elev)).^2)*cosd(2*tau)))/2;
alpha=((kH*alphaH)+(kV*alphaV)+(((kH*alphaH)-
(kV*alphaV))*((cosd(Elev)).^2)*cosd(2*tau)))/(2*k);

gamaR=k*(Rrate.^alpha);          % The rain specific attenuation (dB/km)
disp(['Rain specific attenuation=', num2str(gamaR), ' dB/km']);
if Elev >=5
    Ls=(hR-hs)/(sind(Elev));      % slant-path length below the rain height (km)
end
LG=Ls.*cosd(Elev);              % The horizontal projection of the slant path length (km).

% Calculation of the horizontal reduction factor for 0.01% of the time
c=0.78.*sqrt(LG.*gamaR/f);
d=0.38.*(1-exp(-2.*LG));
ro_o1=1/(1+c-d);

% Calculation of the vertical adjustment factor for 0.01% of the time
eta=atand((hR-hs)/LG.*ro_o1);
if eta > Elev
    LR=(LG.*ro_o1)/cosd(Elev);
else
    LR=(hR-hs)/sind(Elev);
end;
abslat=abs(Lat);
if abslat<36
    kye=36-abslat;
else
    kye=0;
end;
e=31.*(1-exp(-Elev/(1+kye)));
fff=sqrt(LR.*gamaR)/f.^2;
vo_o1=1/(1+sqrt(sind(Elev)).*(e.*fff-0.45));

```

```

% Effective path length (km)
LE=LR*vo_o1;

% Rain attenuation at P=0.01% of time (dB)
RAtt01=LE*gamaR;

% Calculation of rain attenuation at different percentages of time
if P >=(1)|| (abs(Lat)>=36)
    beta=0;
elseif P <(1)&& (abs(Lat)<36)&&(Elev>=25)
    beta=-0.005.*(abs(Lat)-36);
else
    beta=-0.005.*(abs(Lat)-36)+1.8-4.25.*sind(Elev);
end
if P >=(0.001) && (P <=5)
    pu=(-1).*(0.655+(0.033.*log(P))-(0.045.*log(RAtt01))-(beta.*(1-P).*sind(Elev)));
    RainAttP=RAtt01.*(P/0.01).^pu;
else error('Percentage of exceedance time should be from 0.001% to 5% for...
predicting the rain attenuation')
end
disp(['Rain attenuation= ', num2str(RainAttP),' dB']);

%-----
% Cloud attenuation
%-----

% Calculation of the principal & secondary relaxation frequencies:
theta=300/T;
eo=77.6+103.3.*(theta-1);
e1=5.48;
e2=3.51;
fp=20.09-142.*(theta-1)+294.*(theta-1)^2; %GHz
fs=590-1500.*(theta-1); %GHz

% Calculation of the complex dielectric permittivity of water:
eta2=(f/fp).*((eo-e1)/(1+(f/fp)^2))+(f/fs).*((e1-e2)/(1+(f/fs)^2));
eta1=((eo-e1)/(1+(f/fp)^2))+((e1-e2)/(1+(f/fs)^2))+e2;
n=(2+eta1)/eta2;

% cloud specific attenuation coefficient ((dB/km)/(g/m^3))
Kl=0.819.*f/(eta2.*(1+n^2));

CAtten=LWC.*Kl/sind(Elev);
disp(['Cloud attenuation= ', num2str(CAtten),' dB']);

```

```

%-----
% Gases attenuation
%-----

% (1) Water vapor

% calculation of the water vapor specific attenuation
th=300/T;
pw=(RH/5.752)*th*(10.^(10-(9.834*th))); % Water vapor density (g/m^3)
rt=288/T;
rp=p/1013;
n1=0.955*rp*(rt.^0.68)+(0.006*pw);
n2=0.735*rp*(rt.^0.5)+(0.0353*(rt.^4)*pw);
Yw=((3.98*n1*exp(2.23*(1-rt)))/((f-22.235).^2)+9.42*(n1.^2))*(1+((f-22)/(f+22)).^2)+...
    ((11.96*n1*exp(0.7*(1-rt)))/(((f-183.31).^2)+11.14*(n1.^2)))+(0.081*n1*exp(6.44*(1-rt)))/...
    (((f-321.226).^2)+(6.29*(n1.^2)))+(3.66*n1*exp(1.6*(1-rt)))/(((f-325.153).^2)+9.22*(n1.^2))+...
    (25.37*n1*exp(1.09*(1-rt)))/((f-380).^2)+(17.4*n1*exp(1.46*(1-rt)))/((f-448).^2)+...
    (844.6*n1*exp(0.17*(1-rt)))/((f-557).^2)*(1+((f-557)/(f+557)).^2)+((290*n1*exp(0.41*(1-t)))/...
    ((f-752).^2)*(1+((f-752)/(f+752)).^2)+((83328*n2*exp(0.99*(1-rt)))/...
    ((f-1780).^2)*(1+((f-1780)/(f+1780)).^2))*((f.^2)*(rt.^2.5)*(pw*10.^(1-5)));
disp(['water vapor specific attenuation= ', num2str(Yw), ' dB/km']);

% calculation of the path length for water vapor contents (km)
conw=1.013/(1+exp((0-8.1)*(rp-0.57)));
hw=1.66*(1+((1.39*conw)/(((f-22.235).^2)+(2.56*conw)))+(3.37*conw)/(((f-183.31).^2)+...
    (4.69*conw)))+(1.5*conw)/(((f-325.1).^2)+(2.89*conw)));

Aw=Yw*hw; %water vapor attenuation in zenith angle path (dB)

% (2) Dry air

% Definitions:
ee1=(rp.^0.0717)*(rt.^(0-1.8132))*exp(0.0156*(1-rp)-1.6515*(1-rt));
ee2=(rp.^0.5146)*(rt.^(0-4.6368))*exp((0-0.1921)*(1-rp)-5.7416*(1-rt));
ee3=(rp.^0.3414)*(rt.^(0-6.5851))*exp(0.2130*(1-rp)-8.5854*(1-rt));
ee4=(rp.^(0-0.0112))*(rt.^(0.0092))*exp((0-0.1033)*(1-rp)-0.0009*(1-rt));
ee5=(rp.^0.2705)*(rt.^(0-2.7192))*exp((0-0.3016)*(1-rp)-4.1033*(1-rt));
ee6=(rp.^0.2445)*(rt.^(0-5.9191))*exp(0.0422*(1-rp)-8.0719*(1-rt));
ee7=(rp.^(0-0.1833))*(rt.^(6.5589))*exp((0-0.2402)*(1-rp)+6.131*(1-rt));
Y54=2.192*(rp.^1.8286)*(rt.^(0-1.9487))*exp(0.4051*(1-rp)-2.8509*(1-rt));
Y58=12.59*(rp.^1.0045)*(rt.^(3.5610))*exp(0.1588*(1-rp)+1.2834*(1-rt));
Y60=15*(rp.^0.9003)*(rt.^(4.1335))*exp(0.0427*(1-rp)+1.6088*(1-rt));
Y62=14.28*(rp.^0.9886)*(rt.^(3.4176))*exp(0.1827*(1-rp)+1.3429*(1-rt));
Y64=6.819*(rp.^1.4320)*(rt.^(0.6258))*exp(0.3177*(1-rp)-0.5914*(1-rt));
Y66=1.908*(rp.^2.0717)*(rt.^(0-4.1404))*exp(0.4910*(1-rp)-4.8718*(1-rt));
ss=(0-0.00306)*(rp.^3.211)*(rt.^(0-14.94))*exp(1.583*(1-rp)-16.37*(1-rt));

```

```

% Calculation of the dry air specific attenuation
if f<=54
Yo=((7.2*(rt.^2.8))/(f.^2+(0.34*(rp.^2)*(rt.^1.6)))+(0.62*ee3)/((54-...
f).(1.16*ee1)+(0.83*ee2)))*((f.^2)*(rp.^2)*(10.^(0-3)));
elseif f>54 && f<=60
Yo=exp(((log(Y54)./24)*(f-58)*(f-60))-((log(Y58)./8)*...
(f-54)*(f-60))+((log(Y60)./12)*(f-54)*(f-58)));
elseif f>60 && f<=62
Yo=Y60+((Y62-Y60)*((f-60)/2));
elseif f>62 && f<=66
Yo=exp(((log(Y62)./8)*(f-64)*(f-66))-((log(Y64)./4)*(f-62)*...
(f-66))+((log(Y66)./8)*(f-62)*(f-64)));
elseif f>66 && f<=120
Yo=((3.02*(10.^(0-4))*(rt.^3.5))+((0.283*(rt.^3.8)))/((f-...
118.75).^2+(2.91*(rp.^2)*(rt.^1.6)))+...
((0.502*ee6*(1-(0.0163*ee7*(f-66)))/((f-66).^(1.4346*ee4))+...
(1.15*ee5)))*((f.^2)*(rp.^2)*(10.^(1-4)));
elseif f>120 && f<=350
Yo=((3.02*(10.^(0-4)))/(1+(1.9*(10.^(0-5))*(f.^1.5)))+...
((0.283*(rt.^0.3))/((f-118.75).^2+(2.91*(rp.^2)*...
(rt.^1.6)))))*((f.^2)*(rp.^2)*(rt.^3.5)*(10.^(0-3)))+ss;
end
disp(['Dry air specific attenuation= ', num2str(Yo), ' dB/km']);

% Calculation of the equivalent height
t1=(4.64/(1+(0.066*(rp.^(0-2.3))))) * exp(0-((f-59.7)/(2.87+(12.4*exp((0-7.9)*rp))))).^2);
t2=(0.14*exp(2.12*rp))/((f-118.75).^2+0.031*exp(2.2*rp));
t3=(0.0114/(1+(0.14*(rp.^(0-2.6))))) * f * ((0-0.0247+(0.0001*f)+...
(1.61*(10.^(0-6))*f.^2)/(1-(0.0169*f)+(4.1*(10.^(0-5))*f.^2)+(3.2*(10.^(0-7))*f.^3)));
ho=(6.1/(1+(0.17*(rp.^(0-1.1))))) * (1+t1+t2+t3);

Ao=Yo*ho; % Dry air attenuation in zenith angle path (dB)

% Total gases attenuation

Ytot=(Yo+Yw)/sin(Elev);
disp(['Total gases specific attenuation= ', num2str(Ytot), ' dB/km']);
Atot=(Ao+Aw)/sin(Elev);
disp('=====');

%-----
% Extended model
%-----

disp('Extended model!');
disp('=====');
disp('Other Input parameters:');
command = 'Input the bit rate (kb/s): ';
brate = input(command)*1000;

```

```
command = 'Input the noise spectral density: ';
No = input(command);
command = 'Input total system losses (dB) : ';
Ls = input(command);

% Calculating the free space loss (FSL)
lambda=(3*1e8)/(f*10^9);
fsl= 20*log10((4*pi*3.6*1e7)/lambda);
disp(['Free space Loss = ', num2str(fsl), ' dB']);

command = 'Input the atmospheric loss (dB) : ';
La = input(command);
% Here you can define the atmospheric loss (La) according to the specified scenario,
% or you can use the outputs from the aforementioned models.
% Error rate mathematical model can be added as mentioned in section 3.

% Quality indication: Calculating the bit energy to noise ratio
Rpower=EIRP+gr-fsl-La-Ls; % received power (dBW)
ebnor=Rpower-No-10*log10(brate);
disp(['Eb/No = ', num2str(ebnor), ' dB']);

%-----
```

## Acknowledgements

Ministry of Higher Education (MoHE) in Malaysia is thankfully acknowledged for the grant with code ERGS/1-2012/5527096.

## Author details

Ali Mohammed Al-Saegh<sup>1</sup>, A. Sali<sup>1</sup>, J. S. Mandeep<sup>2</sup>, Alyani Ismail<sup>1</sup>,  
Abdulmajeed H.J. Al-Jumaily<sup>1</sup> and Chandima Gomes<sup>3</sup>

1 Department of Computer and Communication Systems Engineering, Universiti Putra Malaysia, Serdang, Selangor, Malaysia

2 Department of Electrical, Electronic and Systems Engineering, Universiti Kebangsaan Malaysia, Bangi, Selangor, Malaysia

3 Department of Electrical and Electronic Engineering, Universiti Putra Malaysia, Serdang, Selangor, Malaysia

## References

- [1] J. Mandeep and Y. Ng, "Satellite Beacon Experiment for Studying Atmospheric Dynamics," *Journal of Infrared, Millimeter and Terahertz Waves*, vol. 31, pp. 988-994, 2010.
- [2] A. Adhikari, A. Bhattacharya, and A. Maitra, "Rain-Induced Scintillations and Attenuation of Ku-Band Satellite Signals at a Tropical Location," *Geoscience and Remote Sensing Letters, IEEE*, vol. 9, pp. 700-704, 2012.
- [3] M. Zubair, Z. Haider, S. A. Khan, and J. Nasir, "Atmospheric influences on satellite communications," *Przeglad Elektrotechniczny*, vol. 87, pp. 261-264, 2011.
- [4] A. D. Panagopoulos, P. D. M. Arapoglou, and P. G. Cottis, "Satellite communications at KU, KA, and V bands: Propagation impairments and mitigation techniques," *Communications Surveys & Tutorials, IEEE*, vol. 6, pp. 2-14, 2004.
- [5] T. V. Omotosho and C. O. Oluwafemi, "Impairment of radio wave signal by rainfall on fixed satellite service on earth-space path at 37 stations in Nigeria," *Journal of Atmospheric and Solar-Terrestrial Physics*, vol. 71, pp. 830-840, 2009.
- [6] A. M. Al-Saegh, A. Sali, J. S. Mandeep, and A. Ismail, "Extracted atmospheric impairments on earth-sky signal quality in tropical regions at Ku-band," *Journal of Atmospheric and Solar-Terrestrial Physics*, vol. 104, pp. 96-105, 2013.
- [7] R. K. Crane, "Prediction of Attenuation by Rain," *Communications, IEEE Transactions on*, vol.28, pp.1717-1733, Sep 1980.
- [8] I. T. U. ITU, "Propagation data and prediction methods required for the design of Earth-space telecommunication systems.," ed: International Telecommunication Union-Recommendation P.618-11, 2013.
- [9] ITU, "Characteristics of precipitation for propagation modelling.," ed: International Telecommunication Union-Recommendation P.837-6, 2012.
- [10] A. Dissanayake, J. Allnutt, and F. Haidara, "A prediction model that combines rain attenuation and other propagation impairments along Earth-satellite paths," *Antennas and Propagation, IEEE Transactions on*, vol. 45, pp. 1546-1558, 1997.
- [11] W. L. Stutzman and W. K. Dishman, "A simple model for the estimation of rain-induced attenuation along earth-space paths at millimeter wavelengths," *Radio Sci.*, vol. 17, pp. 1465-1476, 1982.
- [12] ITU, "Specific attenuation model for rain for use in prediction methods ", ed: International Telecommunication Union-Recommendation P.838-3, 2005.
- [13] S. D. A. Adhikari, A. Bhattacharya, and A. Maitra, "Improving rain attenuation estimation: modelling of effective path length using ku-band measurements at a tropical location," *Progress In Electromagnetics Research B*, vol. 34, pp. 173-186, 2011.

- [14] E. Salonen and S. Uppala, "New prediction method of cloud attenuation," *Electronics Letters*, vol. 27, pp. 1106-1108, 1991.
- [15] I. T. U. ITU, "Attenuation due to clouds and fog.," ed: International Telecommunication Union-Recommendation P.840, 2012.
- [16] A. Dissanayake, J. Allnutt, and F. Haidara, "Cloud attenuation modelling for SHF and EHF applications," *International Journal of Satellite Communications*, vol. 19, pp. 335-345, 2001.
- [17] E. E. Altshuler and R. A. Marr, "Cloud attenuation at millimeter wavelengths," *Antennas and Propagation, IEEE Transactions on*, vol. 37, pp. 1473-1479, 1989.
- [18] L. J. Ippolito, *Satellite communications systems engineering: atmospheric effects, satellite link design and system performance*: Wiley, 2008.
- [19] R. Bhattacharya, R. Das, R. Guha, S. D. Barman, and A. B. Bhattacharya, "Variability of millimetrewave rain attenuation and rain rate prediction: A survey," *Indian Journal of Radio & Space Physics (IJRSP)*, vol. 36, pp. 325-344, Aug-2007 2007.
- [20] A. Maitra and S. Chakraborty, "Cloud Liquid Water Content and Cloud Attenuation Studies with Radiosonde Data at a Tropical Location," *Journal of Infrared, Millimeter and Terahertz Waves*, vol. 30, pp. 367-373, 2009.
- [21] I. T. U. ITU, "Attenuation by atmospheric gases.," ed: International Telecommunication Union-Recommendation P.676-10, 2013.
- [22] V. K. Sakarellos, D. Skraparlis, A. D. Panagopoulos, and J. D. Kanellopoulos, "Outage Performance Analysis of a Dual-Hop Radio Relay System Operating at Frequencies above 10GHz," *Communications, IEEE Transactions on*, vol. 58, pp. 3104-3109, 2010.
- [23] K. K. Teav, Z. Zhendong, and B. Vucetic, "On the Asymptotic Bit Error Probability of M-QAM for MIMO Y Channels," *Communications Letters, IEEE*, vol. 16, pp. 577-580, 2012.
- [24] L. Castanet, M. Bousquet, and D. Mertens, "Simulation of the performance of a Ka-band VSAT videoconferencing system with uplink power control and data rate reduction to mitigate atmospheric propagation effects," *International Journal of Satellite Communications*, vol. 20, pp. 231-249, 2002.
- [25] J. S. Mandeep, S. I. S. Hassan, and K. Tanaka, "Rainfall measurements at Ku-band satellite link in Penang, Malaysia," *Microwaves, Antennas & Propagation, IET*, vol. 2, pp. 147-151, 2008.
- [26] M. K. Simon and M.-S. Alouini, *Digital communication over fading channels*, Second ed. vol. 95. New Jersey: John Wiley & Sons, Inc., 2005.

